To appear in *Remote Sensing Letters*
Vol. 00, No. 00, Month 20XX, 1–8

Revealing the potential of spectral and texture predictor variables in a neural network based rainfall retrieval technique

Hanna Meyer*, Meike Kühnlein, Christoph Reudenbach, Thomas Nauss

Environmental Informatics, Faculty of Geography, Philipps-University Marburg, Deutschhausstr. 10, 35037 Marburg, Germany

(*Received 00 Month 20XX; accepted 00 Month 20XX*)

Estimating rainfall areas and rates from geostationary satellite images has the opportunity of both, a high spatial and a high temporal resolution which cannot be achieved by other satellite-based systems until now. Most recent retrieval techniques base on the spectral channels of the satellites as predictor variables solely. These retrievals can be classified as "purely pixel-based" because no information about the neighbourhood pixels is included. Assuming that precipitation is highly correlated with cloud processes and therefore with cloud texture, texture information derived from the neighbourhood of a pixel might give valuable information about the cloud type and hence about a respective probability of the rainfall rate. To study the potential of texture variables to improve optical rainfall retrieval techniques, rainfall areas and rainfall rates were predicted for Germany 2010 using a neural network approach. In addition to the spectral predictor variables from Meteosat Second Generation (MSG), different grey level co-occurance matrix based texture variables were calculated from all MSG channels. Models were trained for the best performing predictor variables revealed during a recursive feature selection. The performance was then compared to models that used spectral predictors solely. Contrary to expectations, the performance of the models did not increase when texture information were included. Therefore, it could be shown that texture variables have no advantage in machine learning based optical rainfall retrievals over spectral-only models.

1. Introduction

Estimating rainfall from geostationary satellite images has the opportunity of both, a high spatial and a high temporal resolution which cannot be achieved by other satellite-based systems until now. Though recent studies indicate the great potential of optical rainfall retrievals (see valuable overviews by Kidd and Levizzani (2011); Levizzani, Amorati, and Meneguzzo (2002); Levizzani et al. (2001); Prigent (2010); Thies and Bendix (2011)), the task to accurately estimate rainfall from space remains challenging due to the variability of rainfall patterns on the one hand, and due to its high spatio-temporal dynamic on the other.

The majority of recent optical rainfall retrievals base on machine learning algorithms to relate the spectral satellite information to rainfall areas or rainfall rates rather than using parametric approaches (Capacci and Conway 2005; Grimes et al. 2003; Rivolta et al. 2006; Giannakos and Feidas 2013; Hsu et al. 1997; Hong 2003; Kühnlein et al. 2014a). Though different machine learning algorithms are used in

*Corresponding author. Email: hanna.meyer@geo.uni-marburg.de

different retrieval techniques, Meyer et al. (2016) compared the performances of different ML algorithms for the task at hand and concluded that there is a need to improve retrievals by defining suitable predictor variables rather than optimizing by the choice of the ML algorithm.

Among the recent retrievals, the predominating predictor variables which are used are infrared (IR) channels (Feidas and Giannakos 2012; Behrangi et al. 2009) which are in some studies complemented by visible (VIS), near infrared (NIR) and water vapour (WV) channels as well as various channel differences (Kühnlein et al. 2014a,b; Thies, Nauss, and Bendix 2008a,b; Ba and Gruber 2001). These retrievals can be classified as "purely pixel-based" because each pixel in an image is treated completely independent from its neighborhood since no information about the surrounded pixels is included. However, texture information derived from the neighbourhood of a pixel might give valuable information about the cloud type and, due to corresponding microphysical proceses, about a respective probability of the rainfall rate. Texture measures of cloud surfaces in different spatial pixel environments were repeatedly used as proxy for the cloud type (Christodoulou, Michaelides, and Pattichis 2003; Ameur et al. 2004; Welch, Sengupta, and Chen 1988; Giannakos and Feidas 2013), see also a review by Tapakis and Charalambides (2013). Kidd and Levizzani (2011) for example describe stratus clouds as appearing smooth in a certain VIS environment while convective clouds tend to have a heterogeneous surface in the VIS as well as in the IR (Christodoulou, Michaelides, and Pattichis 2003).

Grey level co-occurance matrix (GLCM) based texture measures by Haralick, Shanmugam, and Dinstein (1973) indicate the spatial distribution of grey values in a specific environment and are commonly used in remote sensing of clouds. Welch, Sengupta, and Chen (1988) and Christodoulou, Michaelides, and Pattichis (2003) used the GLCM based texture metrics for cloud classification using Landsat and Meteosat 7 images respectively. Some studies also successfully included GLCM based texture parameters in optical rainfall retrieval techniques (Uddstrom and Gray 1996; Liu et al. 2014; Giannakos and Feidas 2011, 2012; Hong et al. 2004; Hsu et al. 1997). However, in these retrievals, texture is used from IR channel derived brightness temperatures in 3x3 pixel environments solely, or/and the study base on a very limited number of scenes. An extended study on the predictive contribution of texture information using the full spectral information of optical satellite data is still lacking.

Against the background that satellite-based rainfall estimation is still a challenging task, the aim of this study is to analyze the potential of texture variables in different spectral ranges for an improvement of optical rainfall retrieval techniques.

2. Methods

Rainfall areas and rainfall rates were predicted for Germany at the example of the year 2010. Therefore, Meteosat Second Generation (MSG) Spinning Enhanced Visible and Infrared Imager (SEVIRI) data were used since they permit a quasi-continuous observation of the rainfall distribution and rainfall rate in near-real time. A radar-based precipitation product from the German Weather Service, RADOLAN RW (Bartels et al. 2004), was used for ground truth data.

The general retrieval process was two-fold and consists of (i) the identification of precipitating cloud areas and (ii) the assignment of rainfall rates. Since the focus of

this study is on revealing the potential of texture variables, the validation of rainfall rate assignments was based on rainfall areas derived from RADOLAN RW rather than from the results from step (i). This ensures that the performance of rainfall rate models is comparable without confusion based on errors from the prior rainfall areas delineation. Due to unavailability of visible channels during night, rainfall areas and rates were modeled for day and nigh scenes separately.

For all prediction tasks (rainfall areas during day, rainfall areas during night, rainfall rate during day, rainfall rate during night), models were compared that use spectral and texture variables or spectral variables only (Fig. 1). The following sections describe the steps towards a model comparison in detail.

2.1. *Satellite and ground truth data*

MSG SEVIRI (Aminou, Jacquet, and Pasternak 1997) scans the full disk every 15 minutes with a spatial resolution of 3 by 3 km at sub-satellite point. 11 channels measure reflected and emitted radiances at visible, near-infrared and thermal infrared wavelengths. In this study, SEVIRI data from the year 2010 were preprocessed and cloud-masked according to Kühnlein et al. (2014b) and afterwards available on an hourly basis. All 11 MSG channels available during day were used as predictor variables. During night, the three channels in the VIS and NIR were not used since they don't provide reliable information. In addition to the spectral channels, channel differences (Δ T6.2 - 10.8, Δ T6.2 - 10.8,Δ T7.3 - 12.1, Δ T7.3 - 12.1, Δ T8.7 - 10.8, Δ T8.7 - 10.8, Δ T10.8 - 12.1, Δ T10.8 - 12.1, Δ T3.9 - 7.3, Δ T3.9 - 7.3, Δ T3.9 - 10.8, Δ T3.9 - 10.8) were calculated according to Kühnlein et al. (2014a) resulting in 17 spectral varibles during day and 14 spectral variables during night. The GLCM based metrics homogeneity, contrast, dissimilarity, entropy and second moment (Haralick, Shanmugam, and Dinstein 1973) were calculated from all spectral predictors in a 3x3 as well as a 5x5 pixel environment using the "glcm" package in R (Zvoleff 2015). To avoid high computational effort, the number of quantization/grey levels was reduced to 128. The GLCM was calculated for four directions and the averages of all directions were taken as final parameters. In addition to the GLCM based indices, the mean, minimum, maximum and standard deviation values in the 3x3 as well as 5x5 pixel environment of all spectral variables were used as further predictors. In total, including the spectral variables, 342 potential predictor variables during day and 266 during night were presented to the models. All predictors were centered and scaled by dividing the values of the mean-centered variables by their standard deviations. Fig. 2 gives an example of the scaled VIS 0.6 μm channel (Fig. 2a) and the corresponding homogeneity (Fig. 2b) as well as entropy (Fig. 2c) in a 5x5 pixel environment.

As ground truth data, the RADOLAN RW data were used. RADOLAN RW is based on measurements with a C-band Doppler radar of 16 German and neighbouring radar stations. Rain intensity adapted Z/R relationships, statistical clutter filtering and shadowing effects are treated within an on-line calibration process. Furthermore, precipitation intensities are adapted with ground-based precipitation measurements. The precipitation product is available at a temporal resolution of one hour covering the entire area of Germany at a spatial resolution of 1 by 1 km (Bartels et al. 2004). RADDOLAN data were re-projected to geos projection and bi-linearly resampled to match the geometry of the SEVIRI data.

2.2. *Compilation of training and test data sets*

Scenes with at least 3000 rainy pixels were designated as precipitation events based on the RADOLAN RW product. Only these scenes were considered for further analysis. The scenes were splitted into day scenes (scenes with a sun zenith angle > 70) and scenes where the visible channels are not reliably available (i. e. night and twilight). All twilight and night scenes are treated equally in this study and are termed "night" in the following. Since model training using several hundred of predictor variables requires a high computation effort as well as a high amount of storage capacity, a selection of training scenes was required. Therefore, 100 rain events during day and 100 rain events during night were randomly selected. The random selection gave 100 rain events from 78 different days during day and from 76 different days during night. All other rain events in the year 2010 were used as testing scenes. From the training scenes 5% of the cloudy pixels were considered for rainfall areas model training. For training of rainfall rates 25% of the rainy pixels according to the RADOLAN RW product were used. Using a subset of data was necessary due to computing capacity. The selection of training pixels was performed using stratified random sampling to account for the distribution of the dataset. The final training dataset consisted of 110920 pixels for rainfall areas training during day and 63896 during night as well as 141931 pixels for rainfall rate training during day and 102384 during night.

2.3. *Neural network training*

Neural networks are a well established method and were shown to perform best in this optical rainfall retrieval technique with a high computation speed which is important considering the high amount of predictors and data points (Meyer et al. 2016). We used a single-hidden-layer neural network, implemented in the "nnet" package (Venables and Ripley 2002) in R.

2.3.1. Recursive feature selection

Though neural networks are known as being able to deal with highly correlated predictor variables, Kuhn and Johnson (2013) have shown that neural networks are not as unaffected by adding non-informative or redundant parameters. Further, from a technical point of view, many predictors result in a high amount of data which cause storage difficulties and increased computation times. Feature selection is a suitable method to take all potential predictor variables into account but overcome the mentioned issues. We used recursive feature elimination according to Guyon et al. (2002) which is implemented in the caret R package (Kuhn 2014a). Recursive feature elimination fits the model first with all predictor variables. It then calculates variable importance according to the weights method of Gevrey, Dimopoulos, and Lek (2003) and removes the least important variables. In the next step, the model is re-calculated with the reduced number of variables. This step is repeated for different tested quantities of variables. The best number and combination of variables is then determined by comparing the performance of the individual models using Receiver Operating Characteristics (ROC) as performance metric for rainfall areas models and R^2 for rainfall rate models.

Since feature selection is very computation time consuming, parameter tuning was reduced to a minimum during feature selection: The number of neurons in the hidden

layer was tuned between 2 and 10 with increment 2; 15 to 30 with increment 5; 40 to 80 with increment 10 and 100 to the number of predictor variables with increment 50. Weight decay was kept constant at 0.05. The extensive tuning study was carried out after the optimal variables were determined. For all steps of variable selection as well as parameter tuning and model training, stratified 10 fold cross-validation was performed to determine the optimal model settings. Thus, the training samples were randomly partitioned into 10 equally sized folds with respect to the distribution of the response variable (i. e. equal distribution of rainy/non rainy cloud pixels and equal distribution of rainfall rates respectively). Models were then fitted by repeatedly leaving one of the folds out. Performance of a model was determined by predicting on the respective held-out fold. The performance metrics from the hold-out iterations were averaged to the overall cross validated model performance for the respective set of tuning values.

2.3.2. Fine tuning and model training

Models using the optimal variables determined by feature selection as well as the spectral-only models were extensively tuned and trained. Weight decay was tuned between 0 and 0.1 with increment 0.02. The number of neurons in the hidden layer was tuned between 2 and the number of predictor variables with increment 2. The performance of ML algorithms suffers when training classes are highly unbalanced. ML algorithms then tend to maximize performance by over-predicting the majority class. This is particularly critical for the prediction task of this study as the intended prediction target (rainy clouds) usually represents the minority class. To overcome problems caused by unbalanced classes (see e. g. Liu et al. (2006)), the optimal probability cut-off from predictive models for rainfall areas delineation was determined based on ROC analysis (Fawcett 2006; Hamel 2009) following the methodology of Kuhn (2014b). We therefore used the threshold from the predicted probabilities as additional tuning parameter in the classification models (tuned between 0 and 0.4 with increment 0.02 and between 0.5 and 1 with increment 0.1). The threshold leading to the minimal distance to a perfect model was used for the final training of the respective model. See Meyer et al. (2016) for further description on this method. The best performing tuning parameters were applied for final model training. The trained models were used to predict rainfall areas and rainfall rates on the testing scenes.

3. Results

The performance of the rainfall areas models first increased with the number of predictor variables, for both, day and night (Fig. 3a). The optimal number of predictor variables was identified to be 20 (ROC = 0.902) for day and 14 for night (ROC = 0.786). Regarding the night model, the performance then dropped down and remained constant from 75 variables on. The day model was not affected by a high amount of predictor variables and the performance remained constant after the optimal ROC value was reached. The rainfall rate models were more affected by the number of predictor variables (Fig. 3b). The performance first increased to its maximum using 30 variables during day ($R^2 = 0.313$) and 14 variables during night ($R^2 = 0.211$) respectively. The R^2 then rapidly decreased in both, the day and the night models.

There were no significant differences between the models which used the optimal variables revealed during feature selection and the models which used spectral variables only (Fig. 4, 5). The average RMSE of rainfall rate prediction during day was 1.09 mm for spectral-only models and 1.08 mm for the spectral+texture model. During night, the average RMSE was 10.2 in both models. Regarding the prediction of rainfall areas, both models had a probability of detection (POD) of 0.70 and a probability of false detection (POFD) of 0.36 during night. During day, the POFD of both, spectral-only as well as spectral+texture models was 0.20. POD was 0.80 in the spectral-only model and 0.81 in the spectral+texture model. There were also no significant differences in the false alarm ratio (FAR).

4. Discussion and Conclusion

The decreasing performance with increasing number of variables showed that a feature reduction is necessary when a high number of predictor variables is presented to the models. In general, the performance of the retrieval is in the same range as indicated by similar studies (Kühnlein et al. 2014b,a; Giannakos and Feidas 2013). Surprisingly, the use of texture variables did not considerably increase the performance of the models. Concerning the delineation of rainfall areas, these findings correspond to those of Giannakos and Feidas (2011). Though Giannakos and Feidas (2012) showed that texture variables can slightly improve estimations of rainfall rate delineations compared to spectral-only models, these findings could not be confirmed by this study. The contradictions might result from the considerable smaller number of training scenes used by Giannakos and Feidas (2012) which have a higher exposure for overfitting.

Though during feature selection many texture variables were selected for the final model, the performance when the models were actually applied on the satellite images did not improve compared to the spectral-only models. The differences between the cross validated performance and the performance when the models were actually applied to the independent scenes might be a matter of slight overfitting. Since the cross validation was not based on a leave-one-scene-out cross validation, the samples have not been completely independent which might explain the difference between cross validated performance and the completely independent performance.

In summary, we could show that texture variables in optical rainfall retrievals could not improve the final performance compared to spectral-only models. Therefore, in order to avoid high computation time it is reasonable to retain the pixel-based approach which requires the spectral channels of the optical satellite system as predictors only.

5. Acknowledgments

This work was financially supported by the Federal Ministry of Education and Research (BMBF) within the IDESSA project (grant no. 01LL1301) which is part of the SPACES-program (Science Partnership for the Assessment of Complex Earth System processes). The authors are grateful to the German Weather Service (DWD) for providing the RADOLAN RW and the EUMETSAT Earth Observation Portal (https://eoportal.eumetsat.int/) for providing the Meteosat dataset.

References

Ameur, Z., S. Ameur, A. Adane, H. Sauvageot, and K. Bara. 2004. "Cloud classification using the textural features of Meteosat images." *Int. J. Remote Sens.* 25 (21): 4491–4503.

Aminou, D. M. A., B. Jacquet, and F. Pasternak. 1997. "Characteristics of the Meteosat Second Generation (MSG) radiometer/imager: SEVIRI." In *Proceedings of SPIE: Sensors, Systems, and Next-Generation Satellites,* No. 3221. 19–31. 3221.

Ba, Mamoudou B., and Arnold Gruber. 2001. "GOES Multispectral Rainfall Algorithm (GMSRA)." *J. Appl. Meteor.* 40: 1500–1514.

Bartels, H., E. Weigl, T. Reich, P. Lang, A. Wagner, O. Kohler, N. Gerlach, and MeteoSolutions GmbH. 2004. *Projekt RADOLAN - Routineverfahren zur Online-Aneichung der Radarniederschlagsdaten mit Hilfe von automatischen Bodenniederschlagsstationen (Ombrometer).* Offenbach: Deutscher Wetterdienst.

Behrangi, Ali, Kuo-lin Hsu, Bisher Imam, Soroosh Sorooshian, and Robert J. Kuligowski. 2009. "Evaluating the Utility of Multispectral Information in Delineating the Areal Extent of Precipitation." *J. Hydrometeorol.* 10 (3): 684–700.

Capacci, D., and B. J. Conway. 2005. "Delineation of precipitation areas from MODIS visible and infrared imagery with artificial neural networks." *Meteorol. Appl.* 12 (04): 291–305.

Christodoulou, Christodoulos I., Silas C. Michaelides, and Constantinos S. Pattichis. 2003. "Multifeature Texture Analysis for the Classification of Clouds in Satellite Imagery." *IEEE Trans. Geosci. Remote Sens.* 41.

Fawcett, T. 2006. "An introduction to ROC analysis." *Pattern Recogn. Lett.* 27: 861–874.

Feidas, Haralambos, and Apostolos Giannakos. 2012. "Classifying convective and stratiform rain using multispectral infrared Meteosat Second Generation satellite data." *Theor. Appl. Climatol.* 108 (3-4): 613–630.

Gevrey, Muriel, Ioannis Dimopoulos, and Sovan Lek. 2003. "Review and comparison of methods to study the contribution of variables in artificial neural network models." *Ecol. Model.* 160 (3): 249–264.

Giannakos, A., and H. Feidas. 2011. "Detection of rainy clouds based on their spectral and textural features on Meteosat multispectral infrared data." In *EUMETSAT Meteorological Satellite Conference,* Oslo, Norway.

Giannakos, A., and H. Feidas. 2012. "Precipitation estimation based on spectral and textural features of Meteosat multispectral infrared data." In *EUMETSAT Meteorological Satellite Conference,* Sopot, Poland.

Giannakos, Apostolos, and Haralambos Feidas. 2013. "Classification of convective and stratiform rain based on the spectral and textural features of Meteosat Second Generation infrared data." *Theor. Appl. Climatol.* 113 (3-4): 495–510.

Grimes, DIF, E Coppola, M Verdecchia, and G Visconti. 2003. "A neural network approach to real-time rainfall estimation for Africa using satellite data." *J. Hydrometeorol.* 4: 1119–1133.

Guyon, Isabelle, Jason Weston, Stephen Barnhill, and Vladimir Vapnik. 2002. "Gene Selection for Cancer Classification using Support Vector Machines." 46 (1-3): 389–422.

Hamel, Lutz. 2009. *Model Assessment with ROC Curves.* chap. 204, 1316–1323. 2nd ed. Hershey: Information Science Reference (an imprint of IGI Global).

Haralick, R.M., K. Shanmugam, and I. Dinstein. 1973. "Textural Features for Image Classification." 3: 610–621.

Hong, Y. 2003. "Precipitation Estimation from Remotely Sensed Imagery Using an Artificial Neural Network Cloud Classification System." Ph.D. thesis. University of Arizona.

Hong, Yang, Kuo-Lin Hsu, Soroosh Sorooshian, and Xiaogang Gao. 2004. "Precipitation Estimation from Remotely Sensed Imagery Using an Artificial Neural Network Cloud Classification System." *J. Appl. Meteor.* 43 (12): 1834–1853.

Hsu, Kou-lin, Xiaogang Gao, Soroosh Sorooshian, and Hoshin V. Gupta. 1997. "Precipitation Estimation from Remotely Sensed Information Using Artificial Neural Networks." *J. Appl. Meteor.* 36 (9): 1176–1190.

Kidd, C., and V. Levizzani. 2011. "Status of satellite precipitation retrievals." *Hydrol. Earth Syst. Sci.* 15 (4): 1109–1116.

Kuhn, Max. 2014a. *caret: Classification and Regression Training*. R package version 6.0-29. http://CRAN.R-project.org/package=caret.

Kuhn, Max. 2014b. "Optimizing probability thresholds for class imbalances." http://www.r-bloggers.com/optimizing-probability-thresholds-for-class-imbalances/.

Kuhn, Max, and Kjell Johnson. 2013. *Applied Predictive Modeling*. 1st ed. New York: Springer.

Kühnlein, M., T. Appelhans, B. Thies, and T. Nauss. 2014a. "Improving the accuracy of rainfall rates from optical satellite sensors with machine learning - A random forests-based approach applied to MSG SEVIRI." *Remote Sens. Environ.* 141: 129–143.

Kühnlein, Meike, Tim Appelhans, Boris Thies, and Thomas Nauss. 2014b. "Precipitation Estimates from MSG SEVIRI Daytime, Nighttime, and Twilight Data with Random Forests." *J. Appl. Meteor. Climatol.* 53 (11): 2457–2480.

Levizzani, V, R. Amorati, and F. Meneguzzo. 2002. *A Review of Satellite-based Rainfall Estimation Methods*. Technical report. European Commission Project MUSIC Report (EVK1-CT-2000-00058).

Levizzani, V, J Schmetz, H J Lutz, J Kerkmann, P P Alberoni, and M Cervino. 2001. "Precipitation estimations from geostationary orbit and prospects for METEOSAT Second Generation." *Meteorol. Appl.* 8 (1): 23–41.

Liu, Yang, Nitesh V. Chawla, Mary P. Harper, Elizabeth Shriberg, and Andreas Stolcke. 2006. "A study in machine learning from imbalanced data for sentence boundary detection in speech." *Computer Speech & Language* 20 (4): 468–494.

Liu, Yu, Du-Gang Xi, Zhao-Liang Li, and Chun-Xiang Shi. 2014. "Analysis and Application of the Relationship between Cumulonimbus (Cb) Cloud Features and Precipitation Based on FY-2C Image." *Atmosphere* 5 (2): 211–229.

Meyer, H., M. Kühnlein, T. Appelhans, and T. Nauss. 2016. "Comparison of four machine learning algorithms for their applicability in satellite-based optical rainfall retrievals." *Atmos. Res.* 169, Part B: 424–433.

Prigent, Catherine. 2010. "Precipitation retrieval from space: An overview." *C. R. Geosci.* 342: 380–389.

Rivolta, G., F. S. Marzano, E. Coppola, and M. Verdecchia. 2006. "Artificial neural-network technique for precipitation nowcasting from satellite imagery." *Adv. Geosci.* 7: 97–103.

Tapakis, R., and A.G. Charalambides. 2013. "Equipment and methodologies for cloud detection and classification: A review." *Solar Energy* 95: 392 – 430.

Thies, B., and Jrg Bendix. 2011. "Satellite based remote sensing of weather and climate: recent achievements and future perspectives." *Meteorol. Appl.* 18 (3): 262–295.

Thies, B., T. Nauss, and J. Bendix. 2008a. "Discriminating raining from non-raining clouds at mid-latitudes using meteosat second generation daytime data." *Atmos. Chem. Phys.* 8 (9): 2341–2349.

Thies, Boris, Thomas Nauss, and Jörg Bendix. 2008b. "Precipitation process and rainfall intensity differentiation using Meteosat Second Generation Spinning Enhanced Visible and Infrared Imager data." *J. Geophys. Res.: Atmospheres* 113 (D23): n/a–n/a.

Uddstrom, Michael J., and Warren R. Gray. 1996. "Satellite Cloud Classification and Rain-Rate Estimation Using Multispectral Radiances and Measures of Spatial Texture." *J. Appl. Meteor.* 35 (6): 839–858. http://dx.doi.org/10.1175/1520-0450(1996)035¡0839:SCCARR¿2.0.CO;2.

Venables, W. N., and B. D. Ripley. 2002. *Modern Applied Statistics with S*. 4th ed. New York: Springer.

Welch, R. M., S. K. Sengupta, and D. W. Chen. 1988. "Cloud field classification based upon high spatial resolution textural features: 1. Gray level co-occurrence matrix approach." *J. Geophys. Res.: Atmospheres* 93 (D10): 12663–12681.

Zvoleff, Alex. 2015. *glcm: Calculate textures from grey-level co-occurrence matrices (GLCMs) in R*. R package version 1.2. http://CRAN.R-project.org/package=glcm.

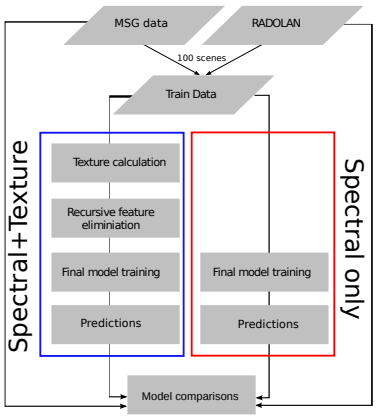

Figure 1. Overview of the methods to compare models that use spectral and texture variables with models that use spectral variables only.

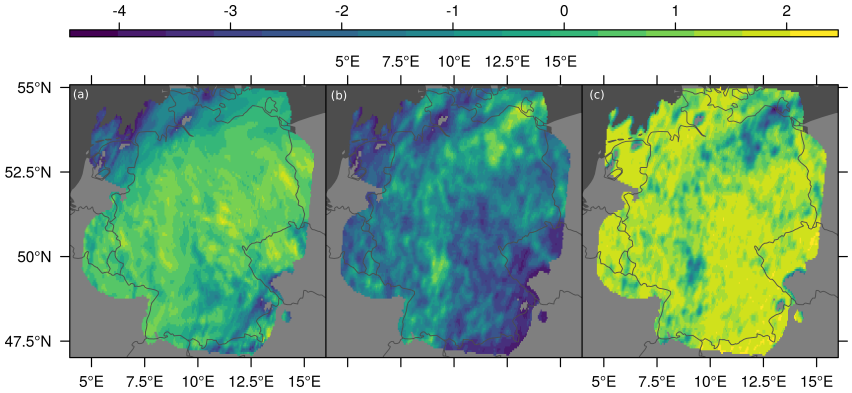

Figure 2. Example of the scaled VIS 0.6 μm channel (a) at 2010/05/06 14:45 as well as the corresponding homogeneity (b) and entropy (c) in a 5x5 pixel environment. Transparent pixels were not cloudy at this time.

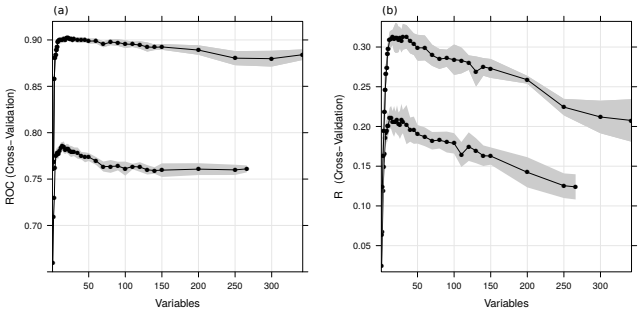

Figure 3. Dependence of the number of variables on the performance of (a) rainfall rates during day (upper line) and night (lower line) incicated by R^2 and of (b) rainfall areas during day (upper line) and night (lower line) indicated by ROC. The grey areas show the standard error.

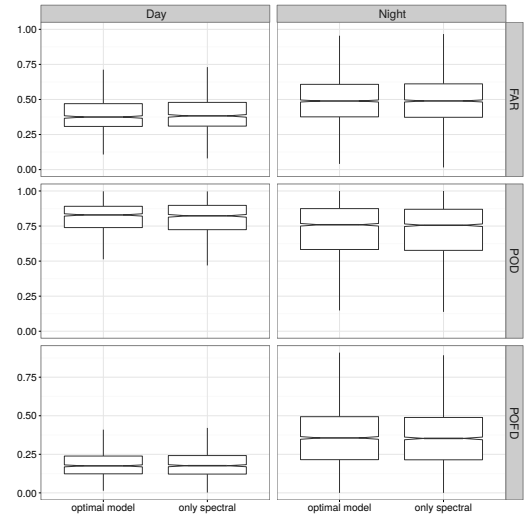

Figure 4. Boxplots showing the performance of the full models as well as spectral-only models for rainfall areas. Note that outliers are excluded since a visual assessment of the differences between models was impossible when a large span of values was illustrated.

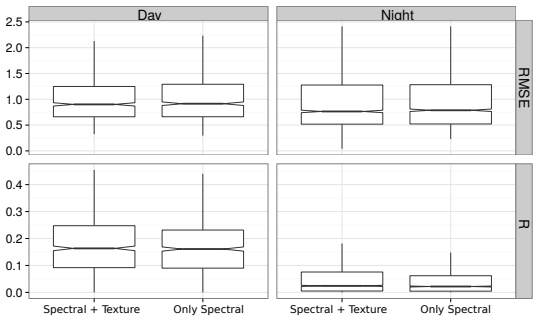

Figure 5. Boxplots showing the performance of the full models as well as spectral-only models for rainfall rates. Note that outliers are excluded since a visual assessment of the differences between models was impossible when a large span of values was illustrated.